Comparative Study of $LiNi_{0.5}Mn_{1.5}O_{4-\delta}$ and $LiNi_{0.5}Mn_{1.5}O_4$ Cathodes Having Two Crystallographic Structures: $Fd\bar{3}m$ and $P4_332$

J.-H. Kim,[†] S.-T. Myung,[‡,§] C. S. Yoon,[∥] S. G. Kang,[∥] and Y.-K. Sun*,[†]

Department of Chemical Engineering and Division of Materials Science and Engineering, Hanyang University, Seungdong-Gu, Seoul 133-791, Republic of Korea, and Department of Chemical Engineering, Iwate University, Iwate 020-8551, Japan

Received October 21, 2003. Revised Manuscript Received December 29, 2003

Nonstoichiometric $LiNi_{0.5}Mn_{1.5}O_{4-\delta}$ and stoichiometric $LiNi_{0.5}Mn_{1.5}O_4$ cathodes with two different structures ($Fd\bar{3}m$ and $P4_332$) were synthesized by a molten salt method. Rietveld refinement of the X-ray diffraction (XRD) data and a selected-area electron diffraction (SAED) study confirmed that the face-centered spinel ($Fd\bar{3}m$) transformed to the primitive simple cubic ($P4_332$) upon additional heating at 700 °C. The $LiNi_{0.5}Mn_{1.5}O_{4-\delta}$ cathode having the space group of $Fd\bar{3}m$ showed better electrochemical behaviors than did the $LiNi_{0.5}Mn_{1.5}O_4$ cathode with the space group of $P4_332$, specifically, a lower area-specific impedance (ASI) and a higher discharge capacity during cycling at high rate. XRD and SAED showed that both stoichiometric and nonstoichiometric $LiNi_{0.5}Mn_{1.5}O_{4-\delta}$ exhibited similar SAED patterns with extra 002 spots at the fully delithiated state, suggesting a structural transition arising from the possible migration of transition metal cations during Li extraction. In addition, stoichiometric $LiNi_{0.5}Mn_{1.5}O_4$ ($P4_332$) had an intermediate phase of $Fd\bar{3}m$ during Li extraction. Such a two-step phase transition of stoichiometric $LiNi_{0.5}Mn_{1.5}O_4$ ($P4_332$) induced low structural reversibility at a high rate (3C rate). Meanwhile, nonstoichiometric $LiNi_{0.5}Mn_{1.5}O_{4-\delta}$ ($Fd\bar{3}m$) exhibited good structural reversibility, as confirmed by XRD and SAED for the cycled electrode even at high rate (3C rate).

Introduction

Recently, several research groups have reported transition-metal-substituted spinel materials ($LiM_xMn_{2-x}O_4$, M = Cr, Co, Fe, Ni, Cu) with high-voltage plateaus at around 5 V.[1−8] The capacities and voltage plateaus in $Li/LiM_xMn_{2-x}O_4$ cells strongly depend on the type of transition metals (M) and their content. Among those materials, $LiNi_{0.5}Mn_{1.5}O_4$ is of special interest for its high discharge capacity and dominant plateau at around 4.7 V, whereas other materials have exhibited two plateaus at around 4.0 and 5 V.[2]

Terada et al.[9] revealed that the plateau at around 4.7 V is due to the Ni^{2+}/Ni^{4+} redox, whereas the plateau at 4.3 V arises from the Mn^{3+}/Mn^{4+} redox couple, as observed by in situ X-ray absorption fine-structure spectroscopy (XAFS) analysis for the $Li_{1-x}Ni_{0.31}Mn_{1.69}O_4$ material. For the ideal $LiNi^{2+}{}_{0.5}Mn^{4+}{}_{1.5}O_4$ composition, the oxidation state of Mn should be fixed at +4, resulting in only the Ni^{2+}/Ni^{4+} redox couple during the charge/discharge process. During the synthesis of the $LiNi_{0.5}Mn_{1.5}O_4$, however, the high calcination temperature sometimes leads to the reduction of the Mn oxidation state from +4 to +3.[2,10] Mn^{3+} participates in the redox, and this, in turn, results in the plateau at around 4 V on charge and discharge.[2,5] Ohzuku et al.[11] employed an annealing process at 700 °C in air after the high-temperature calcination at temperatures as high as 1000 °C. The resulting powders delivered flat voltage profiles at around 4.7 V. Idemoto et al.[10] reported that $LiNi_{0.5}Mn_{1.5}O_4$ synthesized under O_2 atmosphere has the cubic spinel structure with a space group of $P4_332$ instead of $Fd\bar{3}m$, as determined by

* Corresponding author. Phone: +82-2-2290-0524. Fax: +82-2-2282-7329. E-mail: yksun@hanyang.ac.kr.
[†] Department of Chemical Engineering, Hanyang University.
[‡] Iwate University.
[§] Current address: VK Corporation, 67 Jije-Dong, Pyongtaek-City, Kyonggi-do, Republic of Korea.
[∥] Division of Materials Science and Engineering, Hanyang University.

(1) Amine, K.; Tukamoto, H.; Yasuda, H.; Fujita, Y. *J. Electrochem. Soc.* **1996**, *143*, 1607.
(2) Zhong, Q.; Bonakdarpour, A.; Zhang, M.; Gao, Y.; Dahn, J. R. *J. Electrochem. Soc.* **1997**, *144*, 205.
(3) Sigala, C.; Le Gal La Salle, A.; Piffard, Y.; Guyomard, D. *J. Electrochem. Soc.* **2001**, *148*, A812.
(4) Sigala, C.; Le Gal La Salle, A.; Piffard, Y.; Guyomard, D. *J. Electrochem. Soc.* **2001**, *148*, A819.
(5) Sigala, C.; Le Gal La Salle, A.; Piffard, Y.; Guyomard, D. *J. Electrochem. Soc.* **2001**, *148*, A826.
(6) Shigemura, H.; Sakaebe, H.; Kageyama, H.; Kobayashi, H.; West, A. R.; Kanno, R.; Morimoto, S.; Nasu, S.; Tabuchi, M. *J. Electrochem. Soc.* **2001**, *148*, A730.
(7) Strobel, P.; Ibarra Palos, A.; Anne, M.; Le Cras, F. *J. Mater. Chem.* **2000**, *10*, 429.
(8) Kim, J.-S.; Vaughey, J. T.; Johnson, C. S.; Thackeray, M. M. *J. Electrochem. Soc.* **2003**, *150*, A1498.
(9) Terada, Y.; Yasaka, K.; Nishikawa, F.; Konishi, T.; Yoshio, M.; Nakai, I. *J. Solid-State Chem.* **2001**, *156*, 286.
(10) Idemoto, Y.; Narai, H.; Koura, N. *J. Power Sources* **2003**, *119−121*, 125.
(11) Ohzuku, T.; Ariyoshi, K.; Yamamoto, S. *J. Ceram. Soc. Jpn.* **2002**, *110*, 501.

10.1021/cm035050s CCC: $27.50
Published on Web 02/13/2004

neutron diffraction. From these earlier studies, it is considered that the $LiNi_{0.5}Mn_{1.5}O_4$ structure with a space group of $Fd\bar{3}m$ is changed to $P4_332$ by the annealing process, which readily makes the oxidation state of Mn change from +3 to +4, leading to the perfect $LiNi^{2+}{}_{0.5}Mn^{4+}{}_{1.5}O_4$ crystal structure. In this work, we synthesized and compared the structure and electrochemistry of stoichiometric and nonstoichiometirc $LiNi_{0.5}Mn_{1.5}O_{4-\delta}$ having the space groups of $P4_332$ and $Fd\bar{3}m$, respectively.

Experimental Section

Stoichiometric and nonstoichiometric $LiNi_{0.5}Mn_{1.5}O_{4-\delta}$ powders were synthesized by the molten salt method.[12] Stoichiometric amounts of LiOH, $Ni(OH)_2$, and γ-MnOOH (2:1:3) were thoroughly mixed using a Spex mixer/mill and ground again with an excess amount of LiCl salt [Li/(Ni + Mn) = 4.25]. Mixed precursors were calcined at 900 °C for 3 h in a covered alumina crucible. The resulting powders were thoroughly washed with distilled water and ethyl alcohol to remove residual lithium salt and then dried at 110 °C. The nonstoichiometric $LiNi_{0.5}Mn_{1.5}O_{4-\delta}$ powders thus obtained were oxidized to $LiNi_{0.5}Mn_{1.5}O_4$ by annealing at 700 °C for 48 h in air.

Powder X-ray diffraction (XRD, Rint-2000, Rigaku, Tokyo, Japan) measurements using Cu Kα radiation were employed to identify the crystalline phase of the synthesized materials. XRD data were obtained for the range $2\theta = 10-130$ °, with a step size of 0.03 ° and a count time of 5 s. These XRD intensity data were analyzed by Rietveld refinement using Fullprof 2000.[13] Transmission electron microscopy (TEM, JEM2010, JEOL, Tokyo, Japan) was carried out using as-prepared powders and cycled cathodes. The chemical compositions of the resulting powders were analyzed by atomic absorption spectroscopy (AAS, Vario 6, Analytik Jena AG, Jena, Germany). To deduce the average Mn oxidation state, titration with excess sodium oxalate solution using standard $KMnO_4$ was performed.

Electrochemical characterizations were performed using a CR2032 coin-type cell. The cathode was fabricated with 20 mg of $LiNi_{0.5}Mn_{1.5}O_{4-\delta}$ powder and 5 mg of conductive binder (3.3 mg of Teflonized acetylene black and 1.7 mg of graphite). It was pressed on a 200-mm^2 stainless steel mesh used as a current collector and dried at 130 °C for 10 h in a vacuum oven. Lithium foil was used as a negative electrode. The electrolyte solution was 1 M $LiPF_6$ in a mixture of ethylene carbonate (EC) and diethyl carbonate (DEC) in a 1:1 volume ratio (Merck).

Results and Discussion

Structures of $LiNi_{0.5}Mn_{1.5}O_{4-\delta}$ and $LiNi_{0.5}Mn_{1.5}O_4$ Having Different Space Groups: $Fd\bar{3}m$ and $P4_332$. Previous studies have shown that the synthesis of single-phase $LiNi_{0.5}Mn_{1.5}O_4$ is a difficult task; this is largely because of the presence of undesired impurities such as NiO and Li_xNi_yO in the final product, which deteriorates its electrochemical behavior.[1,2,14] To obtain pure $LiNi_{0.5}Mn_{1.5}O_4$ powder, the molten salt method was employed using LiCl−LiOH mixed salts. When the ratio of molten salt to transition metals {(LiOH + LiCl)/[Ni$(OH)_2$ + γ-MnOOH]} was less than 4, the crystallinity of the final product was relatively lower than that obtained with the present ratio (4.25). The resulting

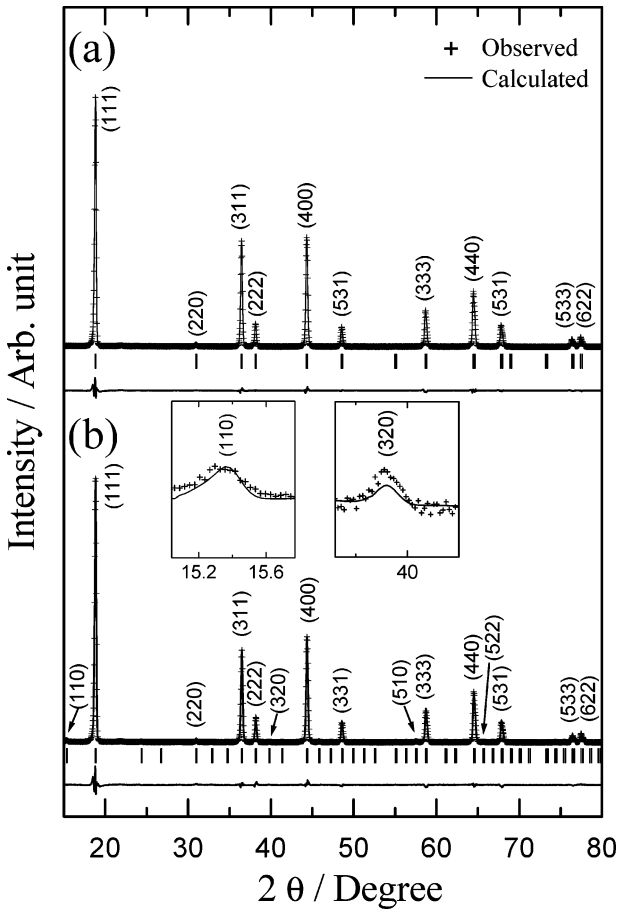

Figure 1. Rietveld refinement profiles of XRD data for (a) $LiNi_{0.5}Mn_{1.5}O_{4-\delta}$ and (b) $LiNi_{0.5}Mn_{1.5}O_4$ powders.

$LiNi_{0.5}Mn_{1.5}O_{4-\delta}$ powder was annealed again at 700 °C for 48 h to oxidize the remaining Mn^{3+} to Mn^{4+} ($LiNi_{0.5}Mn_{1.5}O_4$). From the AAS analysis, the chemical compositions of the two powders were determined to be $Li_{1.00}Ni_{0.5}Mn_{1.50}O_{4-\delta}$ and $Li_{1.00}Ni_{0.50}Mn_{1.50}O_4$. To confirm the oxygen contents in the final products, the oxidation state of Mn was deduced by a redox titration with $KMnO_4$, assuming that the average oxidation state of Ni is +2. The average oxidation states of Mn for $LiNi_{0.5}Mn_{1.5}O_{4-\delta}$ and $LiNi_{0.5}Mn_{1.5}O_4$ were 3.92 and 4.00, respectively, giving rise to the formulas $Li_{1.00}Ni_{0.48}Mn_{1.50}O_{3.92}$ and $Li_{1.00}Ni_{0.50}Mn_{1.50}O_{4.00}$. This result also confirms that the additional heat treatment at 700 °C clearly brought about the oxidation of Mn.

To identify the structures of $LiNi_{0.5}Mn_{1.5}O_{4-\delta}$ and $LiNi_{0.5}Mn_{1.5}O_4$, we performed Rietveld refinements. Figure 1 shows Rietveld refinement patterns of the XRD data for the $LiNi_{0.5}Mn_{1.5}O_{4-\delta}$ and $LiNi_{0.5}Mn_{1.5}O_4$ powders. Both powders exhibited phase-pure cubic spinel structures without impurities such as NiO and Li_xNi_yO. A careful examination revealed that the two XRD patterns were somewhat different. As shown in Figure 1b, small peaks that are considered to represent a superstructure were observed at 15.3 °, 39.7 °, 45.7 °, 57.5 °, and 65.6 ° for $LiNi_{0.5}Mn_{1.5}O_4$, but were absent from pattern of $LiNi_{0.5}Mn_{1.5}O_{4-\delta}$ in Figure 1a. Similar results were previously observed for $LiMg_{0.5}Mn_{1.5}O_4$ and $LiZn_{0.5}Ti_{1.5}O_4$ by Strobel et al.[7] and West et al.,[15]

(12) Yang, X.; Tang, W.; Kanoh, H.; Ooi, K. *J. Mater. Chem.* **1999**, *9*, 2683.
(13) Rodriguez-Carjaval, J. *Physica B* **1993**, *192*, 55.
(14) Alcántara, R.; Jaraba, M.; Lavela, P.; Tirado, J. L. *Electrochim. Acta* **2002**, *47*, 1829.
(15) Kawai, H.; Tabuchi, M.; Nagata, M.; Tukamoto, H.; West, A. R. *J. Mater. Chem.* **1998**, *8*, 1273.

Table 1. Structural Parameters Obtained from Rietveld Refinement of $LiNi_{0.5}Mn_{1.5}O_{4-\delta}$ Based on a Space Group of $Fd\bar{3}m$

atom	Wyckoff position	*x*	*y*	*z*	*B* (Å^2)
Li	8*a*	$^1/_8$	$^1/_8$	$^1/_8$	0.55(10)
Ni	16*d*	$^1/_2$	$^1/_2$	$^1/_2$	0.43(6)
Mn	16*d*	$^1/_2$	$^1/_2$	$^1/_2$	0.43(6)
O	32*e*	0.263(11)	0.263(11)	0.263(11)	1.31(15)

Table 2. Structural Parameters Obtained from Rietveld Refinement of $LiNi_{0.5}Mn_{1.5}O_4$ Based on a Space Group of $P4_332$

atom	Wyckoff position	*x*	*y*	*z*	*B* (Å^2)
Li	8*c*	0.012 90(7)	0.012 90(7)	0.012 90(7)	1.44(6)
Ni	4*a*	$^5/_8$	$^5/_8$	$^5/_8$	2.34(9)
Mn	12*d*	$^1/_8$	0.3791(4)	−0.1291(4)	2.34(9)
O1	8*c*	0.3863(24)	0.3863(24)	0.3863(24)	2.55(17)
O2	24*e*	0.1492(26)	−0.1467(33)	0.1313(38)	2.55(17)

Table 3. Refinement Results for $LiNi_{0.5}Mn_{1.5}O_{4-\delta}$ and $LiNi_{0.5}Mn_{1.5}O_4$ Based on the Two Different Space Groups of $Fd\bar{3}m$ and $P4_332$

sample	space group	*a* (Å)	vol (Å^3)	R_{wp} (%)	R_{Bragg} (%)
$LiNi_{0.5}Mn_{1.5}O_{4-\delta}$	$Fd\bar{3}m$	8.172(4)	545.753(5)	10.3	1.89
$LiNi_{0.5}Mn_{1.5}O_4$	$P4_332$	8.166(3)	544.541(4)	11.5	3.58

respectively. Such extra peaks suggest the occurrence of a phase transformation brought about by annealing at 700 °C. Recent reports have shown that $LiNi_{0.5}Mn_{1.5}O_4$ synthesized under O_2 atmosphere or reoxidized after calcination at temperatures over 900 °C have a space group of $P4_332$.[10,11] When the refinement was performed using the $Fd\bar{3}m$ space group, the sites in which the atoms were assumed to be located were as follows: Li atoms in 8*a* sites, Ni and Mn atoms in 16*d* sites, and O atoms in 32*e* sites. The occupation of the oxygen atoms was also fixed to 1 for the refinement, even though the chemical composition of the sample showed an oxygen deficiency. In addition, the Ni and Mn atoms were assumed to be randomly distributed on 16*d* sites. For the $P4_332$ space group, however, the refinement was done assuming Li atoms to be in 8*c* sites, Ni atoms in 4*a* sites, Mn atoms in 12*d* sites, and O atoms in 8*c* and 24*e* sites. In this case, the Ni and Mn atoms were ordered regularly.[7,15,16] The refinement profiles for the $LiNi_{0.5}Mn_{1.5}O_{4-\delta}$ indicated that all of the peaks fit well to the space group of $Fd\bar{3}m$, as seen in Figure 1a, and the fitted structural parameters and the refined results are listed in Tables 1 and 3.

On the contrary, the stoichiometric $LiNi_{0.5}Mn_{1.5}O_4$ compound was refined assuming the space group of $P4_332$ and a good agreement was seen between the observed and calculated patterns in Figure 1(b) by following structural parameters presented in Table 2. The refinement results appear in Table 3. From these results, it was found that $LiNi_{0.5}Mn_{1.5}O_4$ has an ordered structure of Ni and Mn ions at the 4*a* and 12*d* sites, respectively. From the Rietveld refinement results, it was confirmed that the stoichiometry of $LiNi_{0.5}Mn_{1.5}O_4$ results in different structures with the different space groups of $Fd\bar{3}m$ and $P4_332$ depending on the annealing process after calcination at 900 °C for 3 h.

(16) Blasse, G. *Philips Res. Rep.* **1964**, 1.

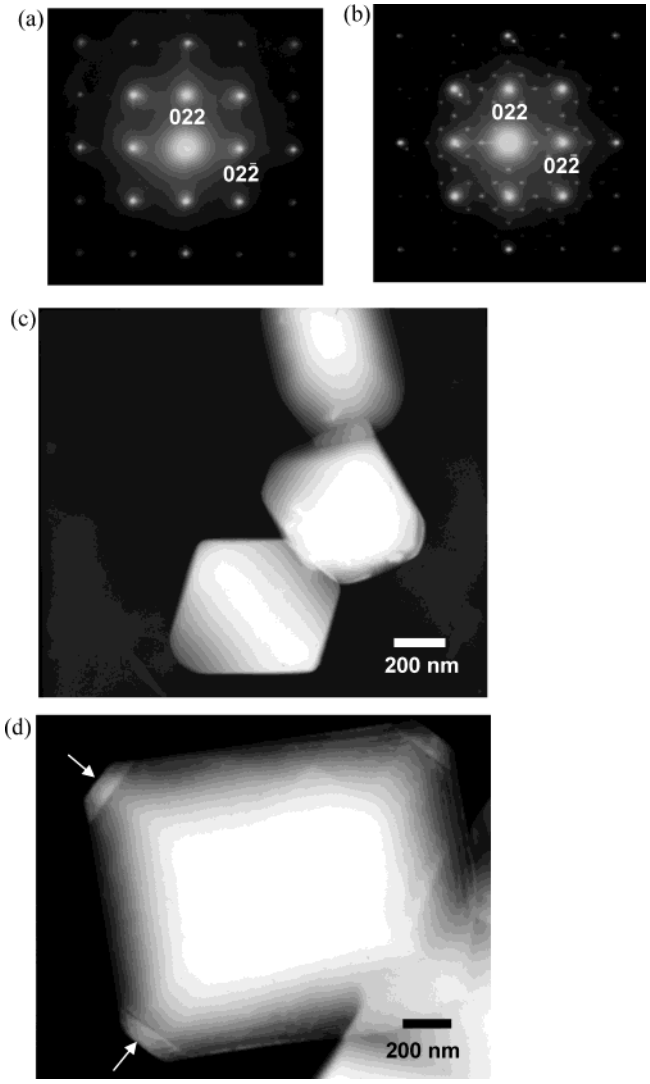

Figure 2. Electron diffraction patterns of (a) $LiNi_{0.5}Mn_{1.5}O_{4-\delta}$ and (b) $LiNi_{0.5}Mn_{1.5}O_4$ phases in the [100] zone and TEM bright-field images of (c) $LiNi_{0.5}Mn_{1.5}O_{4-\delta}$ and (d) $LiNi_{0.5}Mn_{1.5}O_4$ powders. [Spots corresponding to $0k0$ ($00l$) with $k \neq 4n$ ($l \neq 4n$) in part b that should be extinct appear because of the double diffraction.]

To observe the structural differences between the stoichiometric and nonstoichiometric $LiNi_{0.5}Mn_{1.5}O_{4-\delta}$ phases in detail, TEM was used, and the corresponding results are shown in Figure 2. The electron diffraction patterns obtained from two $LiNi_{0.5}Mn_{1.5}O_4$ phases in Figure 2a and b clearly demonstrate the differences in structure. In agreement with the XRD data in Figure 1, $LiNi_{0.5}Mn_{1.5}O_{4-\delta}$ exhibited a typical spinel diffraction pattern in the 100 zone, whereas the diffraction pattern in the same orientation from the annealed powder, $LiNi_{0.5}Mn_{1.5}O_4$, exhibited numerous superlattice peaks in addition to the strong spinel. The extra spots were indexed to the primitive simple cubic structure ($P4_332$). Figure 2c and d shows the TEM bright-field images from the two powders. Both powders exhibited well-developed octahedral shapes, although a secondary phase appeared to grow on the corner of the octahedral particle during annealing, as indicated in Figure 2d, which is usually observed in annealed ceramic powders.

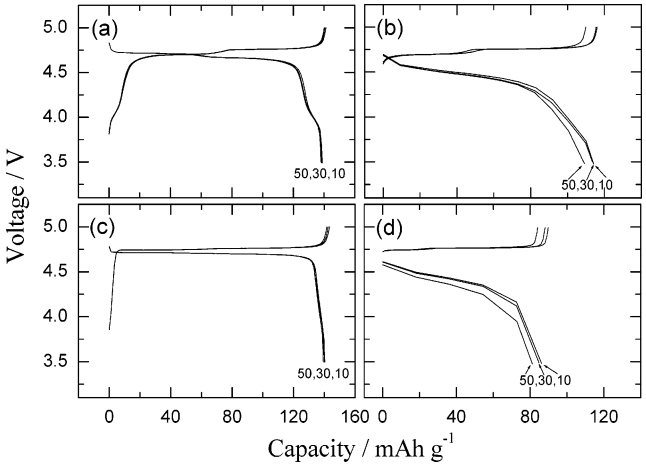

Figure 3. Charge/discharge curves of $LiNi_{0.5}Mn_{1.5}O_{4-\delta}$ and $LiNi_{0.5}Mn_{1.5}O_4$ at the 10th, 30th, and 50th cycles at 30 °C. (a) $LiNi_{0.5}Mn_{1.5}O_{4-\delta}$, $^1/_7$C rate; (b) $LiNi_{0.5}Mn_{1.5}O_{4-\delta}$, 3C rate; (c) $LiNi_{0.5}Mn_{1.5}O_4$, $^1/_7$C rate; and (d) $LiNi_{0.5}Mn_{1.5}O_4$, 3C rate.

Electrochemical Properties of $LiNi_{0.5}Mn_{1.5}O_{4-\delta}$ and $LiNi_{0.5}Mn_{1.5}O_4$ Having Different Space Groups: $Fd\bar{3}m$ and $P4_332$. The electrochemical properties of the stoichiometric and nonstoichiometric $LiNi_{0.5}Mn_{1.5}O_{4-\delta}$ materials were investigated. The charge/discharge profiles between 3.5 and 5 V at 30 °C are shown in Figure 3 a−d. The Li/$LiNi_{0.5}Mn_{1.5}O_{4-\delta}$ and Li/$LiNi_{0.5}Mn_{1.5}O_4$ cells were cycled at a low rate ($^1/_7$C rate) and at a high rate (3C rate). In the case of the low-rate cycling, a constant current density of 20 mA g^{-1} was applied to the cells in Figure 3a and c. For the high-rate cycling, the Li/$LiNi_{0.5}Mn_{1.5}O_{4-\delta}$ and Li/$LiNi_{0.5}Mn_{1.5}O_4$ cells were charged with the same constant current density of 20 mA g^{-1} and discharged at the current density of 325 mA g^{-1} in Figure 3b and d. The Li/$LiNi_{0.5}Mn_{1.5}O_{4-\delta}$ cell shows two distinct plateaus at around 4.7 V (Figure 3a) that are attributed to the $Ni^{2+/4+}$ redox couple.[1,2,17] A small plateau in the 4 V region was also observed that arises from the $Mn^{3+/4+}$ redox couple.[2,9] In the ideal $LiNi_{0.5}Mn_{1.5}O_4$ structure, the oxidation state of manganese is fixed at +4. With increasing calcination temperature, however, an oxygen deficiency appears in $LiNi_{0.5}Mn_{1.5}O_4$, and this partly lowers the manganese oxidation state from Mn^{4+} to Mn^{3+}.[2,18] This means that a small portion of the manganese remained as Mn^{3+} for the Li/$LiNi_{0.5}Mn_{1.5}O_{4-\delta}$ cell. Even though the cycling rate was increased to 3C on discharge, the discharge capacity was 114 mAh g^{-1} at the 10th and 30th cycles, which was about 83% compared to the value of 138 mAh g^{-1} at the $^1/_7$C rate (Figure 3b).

In contrast, the Li/$LiNi_{0.5}Mn_{1.5}O_4$ cell exhibited a flat voltage profile at around 4.7 V and no plateau at the 4 V region (Figure 3c). From the absence of the 4 V plateau, it is thought that the residual Mn^{3+} in $LiNi_{0.5}Mn_{1.5}O_{4-\delta}$ is oxidized to Mn^{4+} by the annealing process. Although the Li/$LiNi_{0.5}Mn_{1.5}O_4$ cell shows a slightly higher discharge capacity of 140 mAh g^{-1} at the $^1/_7$C rate, it exhibited a lower discharge capacity than the Li/ $LiNi_{0.5}Mn_{1.5}O_{4-\delta}$ cell when discharged at the rate

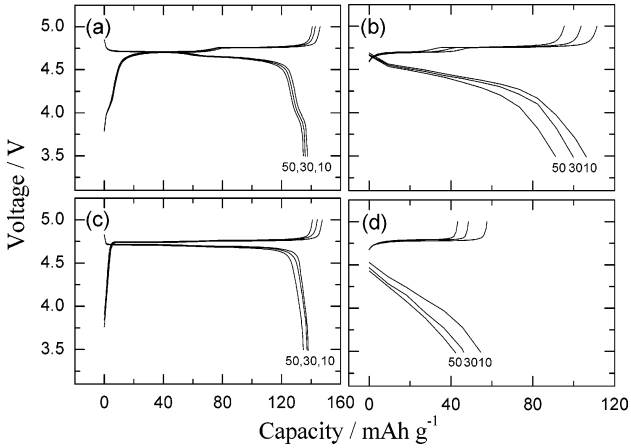

Figure 4. Charge/discharge curves of $LiNi_{0.5}Mn_{1.5}O_{4-\delta}$ and $LiNi_{0.5}Mn_{1.5}O_4$ at the 10th, 30th, and 50th cycles at 55 °C. (a) $LiNi_{0.5}Mn_{1.5}O_{4-\delta}$, $^1/_7$C rate; (b) $LiNi_{0.5}Mn_{1.5}O_{4-\delta}$, 3C rate; (c) $LiNi_{0.5}Mn_{1.5}O_4$, $^1/_7$C rate; and (d) $LiNi_{0.5}Mn_{1.5}O_4$, 3C rate.

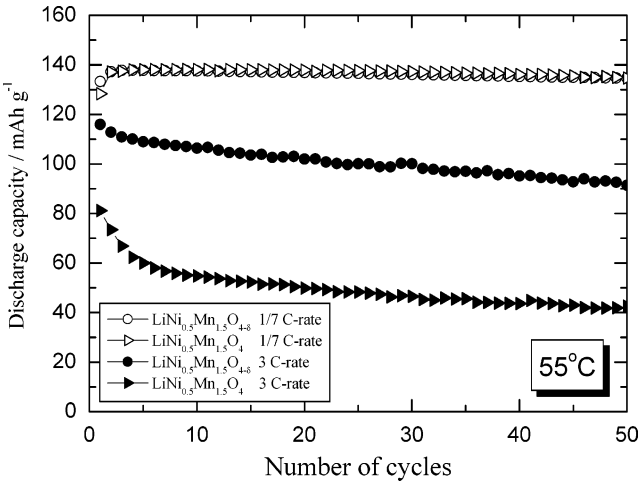

Figure 5. Electrochemical cycling performances of Li/$LiNi_{0.5}Mn_{1.5}O_{4-\delta}$ and Li/$LiNi_{0.5}Mn_{1.5}O_4$ cells at rates of $^1/_7$C and 3C at 55 °C.

of 3C. In this case, the Li/$LiNi_{0.5}Mn_{1.5}O_4$ cell shows a low discharge capacity of 86 mAh g^{-1} at the 10th cycle, which is about 61% of the discharge capacity observed at the rate of $^1/_7$C. At a low current density of 20 mA g^{-1}, which approximately corresponds to the $^1/_7$C rate, the Li/$LiNi_{0.5}Mn_{1.5}O_{4-\delta}$ and Li/$LiNi_{0.5}Mn_{1.5}O_4$ cells exhibit discharge capacities of ca. 140 and 138 mAh g^{-1}, respectively, for 50 cycles. However, when discharged at a rate of 3C, a gradual capacity loss was observed especially for Li/$LiNi_{0.5}Mn_{1.5}O_4$. The capacity retentions were 91 and 84% after 50 cycles for $LiNi_{0.5}Mn_{1.5}O_{4-\delta}$ and $LiNi_{0.5}Mn_{1.5}O_4$, respectively.

Electrochemical performance at 55 °C was also investigated. The charge/discharge profiles show voltage profiles similar to that observed 30 °C at the low rate of $^1/_7$C in Figure 4a−d. At the high rate of 3C on discharge, however, the Li/$LiNi_{0.5}Mn_{1.5}O_{4-\delta}$ cell hardly showed a plateau during discharge and exhibited a low discharge capacity (see Figure 4b). Figure 5 shows the cycling performances for the stoichiometric and nonstoichiometric Li/$LiNi_{0.5}Mn_{1.5}O_{4-\delta}$ cells at 55 °C. The Li/$LiNi_{0.5}Mn_{1.5}O_{4-\delta}$ and Li/$LiNi_{0.5}Mn_{1.5}O_4$ cells exhibited discharge capacities of ca. 136 and 137 mAh g^{-1}, respectively, during 50 cycles at the low rate of $^1/_7$C, and

(17) Mansour, A. N.; Melendres, C. A. *J. Phys. Chem. A* **1998**, *102*, 65.
(18) Myung, S.-T.; Komaba, S.; Kumagai, N.; Yashiro, H.; Chung, H.-T.; Cho, T.-H. *Electrochim. Acta* **2002**, *47*, 2543.

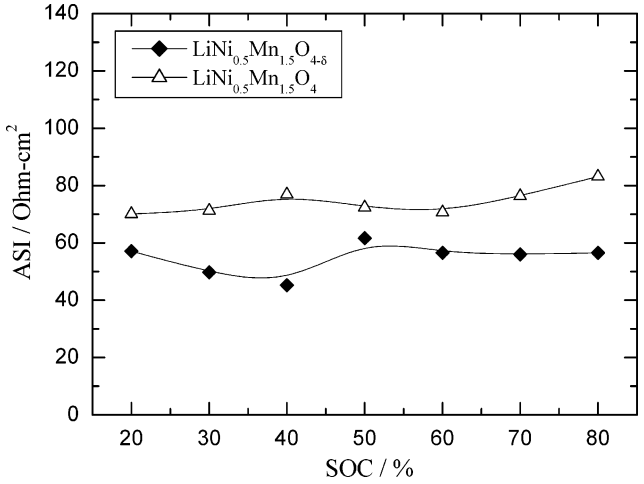

Figure 6. Area-specific impedances (ASIs) of Li/$LiNi_{0.5}Mn_{1.5}O_{4-\delta}$ and Li/$LiNi_{0.5}Mn_{1.5}O_4$ cells as a function of state of charge (SOC).

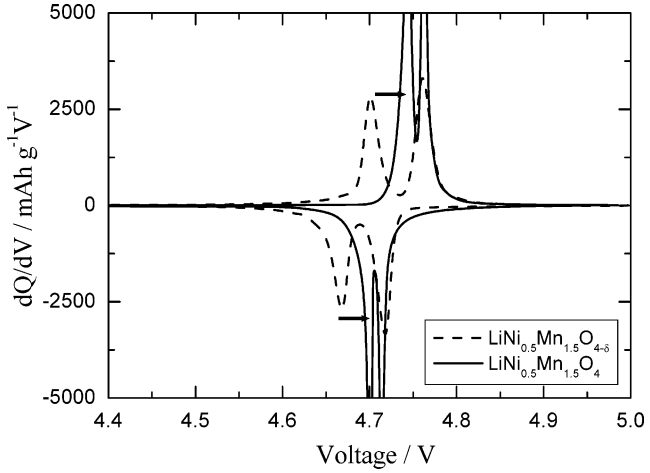

Figure 7. Differential capacity vs voltage curves for the Li/$LiNi_{0.5}Mn_{1.5}O_{4-\delta}$ and Li/$LiNi_{0.5}Mn_{1.5}O_4$ cells between 3.5 and 5 V at a current density of 20 mA g^{-1}.

their capacity retentions were about 98% after 50 cycles. However, both Li/$LiNi_{0.5}Mn_{1.5}O_4$ cells exhibited a rapid capacity fading at the 3C rate on discharge. The Li/$LiNi_{0.5}Mn_{1.5}O_{4-\delta}$ cell still exhibited a higher discharge capacity and better cycling performance than the Li/$LiNi_{0.5}Mn_{1.5}O_4$ cell at the 3C rate. It was initially speculated that $LiNi_{0.5}Mn_{1.5}O_{4-\delta}$ showing the $Mn^{3+/4+}$ redox couple would have relatively poor electrochemical performances because of the presence of Jahn−Teller ions, Mn^{3+}, compared to the $LiNi_{0.5}Mn_{1.5}O_4$, which is considered to have only Mn^{4+} in its oxide matrix. In our case, however, although Mn^{3+} ions are present in $LiNi_{0.5}Mn_{1.5}O_{4-\delta}$ having the $Fd\bar{3}m$ space group, this material shows superior electrochemical performances to $LiNi_{0.5}Mn_{1.5}O_4$ with the space group of $P4_332$ during the high-rate test at both 30 and 55 °C. It is notable that the Li/$LiNi_{0.5}Mn_{1.5}O_{4-\delta}$ cell shows a higher discharge capacity than the Li/$LiNi_{0.5}Mn_{1.5}O_4$ cell at the high rate, which is contrary to the result at the low rate.

To understand the higher discharge capacity of the $LiNi_{0.5}Mn_{1.5}O_{4-\delta}$ ($Fd\bar{3}m$) at high rate, the area-specific impedance (ASI) was measured at 30 °C as a function of the state of charge (SOC). The ASI was determined according to the expression $(A\Delta V)/I$, where A is the cross-sectional area, ΔV is the voltage variation during current interruption for 1 min at each SOC, and I is the current applied during galvanostatic cycling. The $LiNi_{0.5}Mn_{1.5}O_{4-\delta}$ electrode exhibited a lower ASI value than the $LiNi_{0.5}Mn_{1.5}O_4$ electrode, as shown in Figure 6. The $LiNi_{0.5}Mn_{1.5}O_{4-\delta}$ ($Fd\bar{3}m$) and $LiNi_{0.5}Mn_{1.5}O_4$ ($P4_332$) electrodes showed ASI values of ca. 55 and 75 Ω·cm^2, respectively, at 20−80% of SOC.

Structural Investigation of $LiNi_{0.5}Mn_{1.5}O_{4-\delta}$ and $LiNi_{0.5}Mn_{1.5}O_4$ during Cycling. Figure 7 shows dQ/dV curves for Li/$LiNi_{0.5}Mn_{1.5}O_{4-\delta}$ and Li/$LiNi_{0.5}Mn_{1.5}O_4$ cells between 3.5 and 5 V obtained by applying a constant current density of 20 mA g^{-1}. Both cells show two plateaus at around 4.7 V during charge/discharge process. Although the Li/$LiNi_{0.5}Mn_{1.5}O_4$ cell seems to have only one plateau during the charge/discharge process in Figures 3c and 4c, the dQ/dV curve indicates that it also has two plateaus in the 4.7 V region, as shown in Figure 7. Although the upper voltage plateau appears in the same voltage region for the two cells, the lower voltage plateau of the Li/$LiNi_{0.5}Mn_{1.5}O_{4-\delta}$ cell appears at a slightly lower voltage than that of the Li/$LiNi_{0.5}Mn_{1.5}O_4$ cell. As indicated by the arrows, the lower-voltage plateaus were shifted to the higher-voltage region by the phase transformation to $P4_332$: from 4.7 to 4.74 V on charge and from 4.66 to 4.7 V on discharge. Goodenough's group explained a similar phenomenon observed using oxide and sulfide. In that case, the stronger bonding in the oxide than the sulfide resulted in an increase in the redox energy.[19,20] Myung et al.[21] also reported an increase of the redox potential upon substitution of more Al for Mn in $LiAl_xMn_{2-x}O_4$, which would be due to the stronger Al−O bonding than Mn−O. From the increase in the redox potential, it can be suggested that the Li ion requires more energy to be intercalated/deintercalated from the host structure in the case of $LiNi_{0.5}Mn_{1.5}O_4$. The voltage shift to the higher-voltage region of the lower-voltage plateau would be ascribed to the formation of a different structure.

Ex situ XRD patterns for $LiNi_{0.5}Mn_{1.5}O_{4-\delta}$ and $LiNi_{0.5}Mn_{1.5}O_4$ were measured at each state of charge to observe the phase transition during Li^+ deintercalation. The $Li_xNi_{0.5}Mn_{1.5}O_{4-\delta}$ electrode was charged from $x = 1.0$ to $x = 0.04$, and the results are shown in Figure 8. The pristine cubic phase ($x = 0$) was shifted to the higher angle as Li^+ was deintercalated from the $LiNi_{0.5}Mn_{1.5}O_{4-\delta}$ host material, and then another cubic phase appeared when more than 50% of the Li^+ was deintercalated. Finally, at the fully charged state, $Li_{0.04}Ni_{0.5}Mn_{1.5}O_{4-\delta}$ showed the dominant second cubic phase. This result is consistent with the previous report that $LiNi_{0.5}Mn_{1.5}O_4$ with a space group of $Fd\bar{3}m$ undergoes a topotactic two-phase transition during cycling.[14,18] Figure 9 illustrates the changes in the lattice parameter, a, for the $Li_xNi_{0.5}Mn_{1.5}O_{4-\delta}$ at each state of charge (closed symbols). The lattice constant of the pristine cubic phase decreased linearly upon Li^+ extraction from the $Li_xNi_{0.5}Mn_{1.5}O_{4-\delta}$, whereas that of the second cubic phase remained almost constant at around 8 Å.

(19) Goodenough, J. B. *Solid State Ionics* **1994**, *69*, 184.
(20) Manthiram, A.; Goodenough, J. B. *J. Solid State Chem.* **1987**, *71*, 349.
(21) Myung, S.-T.; Komaba, S.; Kumagai, N. *J. Electrochem. Soc.* **2001**, *148*, A482.

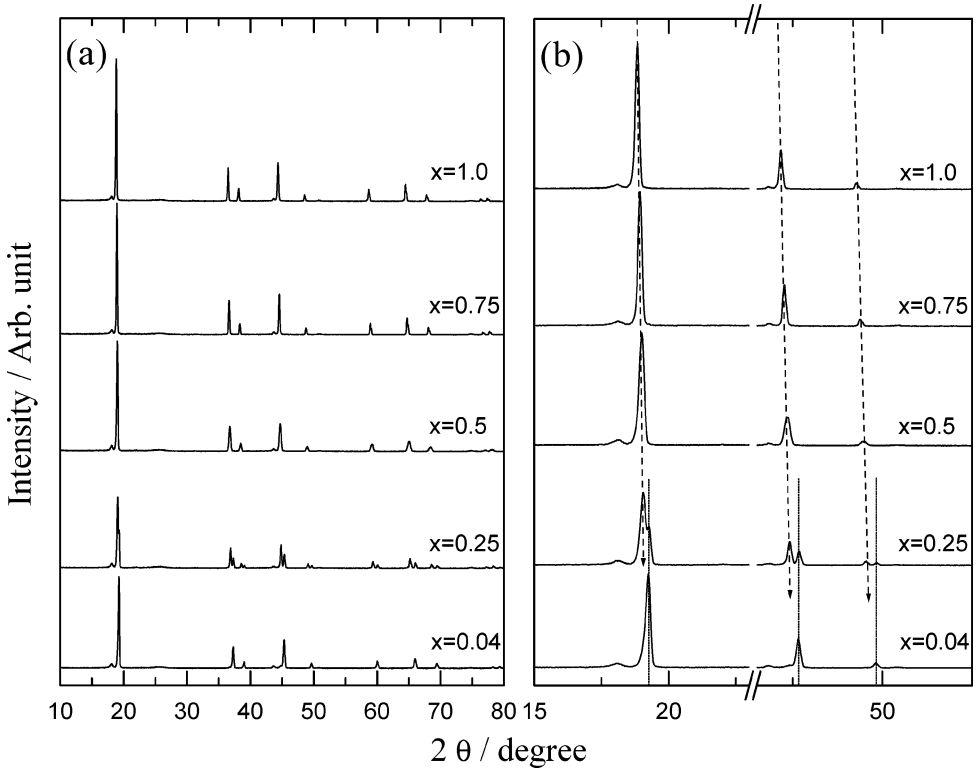

Figure 8. Ex situ X-ray diffraction (XRD) patterns of $Li_xNi_{0.5}Mn_{1.5}O_{4-\delta}$ ($Fd\bar{3}m$) electrodes at different states of charge.

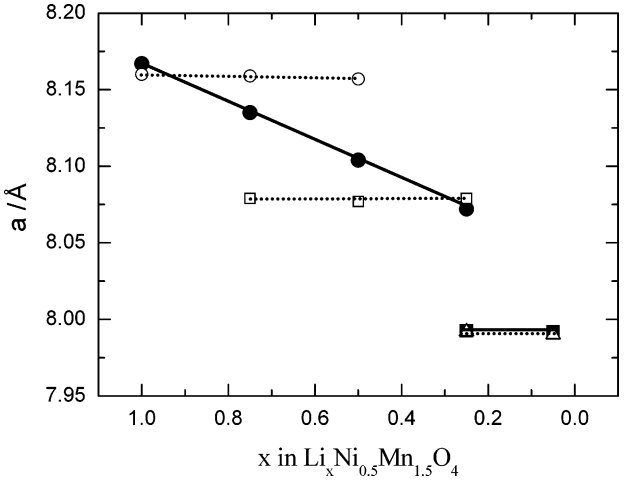

Figure 9. Variation in lattice parameter, a, for $Li_xNi_{0.5}Mn_{1.5}O_{4-\delta}$ (closed symbols) and $Li_xNi_{0.5}Mn_{1.5}O_4$ (open symbols) electrodes on charge.

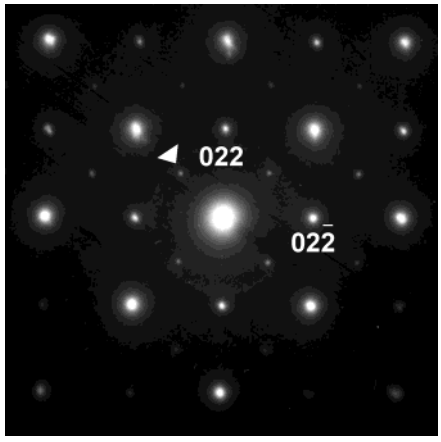

Figure 10. Ex situ electron diffraction patterns in the 100 zone for the $Li_{0.04}Ni_{0.5}Mn_{1.5}O_{4-\delta}$ ($Fd\bar{3}m$) electrode. The arrows indicate the extra 002 spot that should be extinct for the normal $Fd\bar{3}m$ structure.

To observe the structural changes in detail, TEM observations were carried out. The original spinel symmetry was well maintained during Li extraction until the composition of $Li_{0.25}Ni_{0.5}Mn_{1.5}O_4$ was reached. When Li^+ was further extracted to form $Li_{0.04}Ni_{0.5}Mn_{1.5}O_4$, however, faint spots were observed that could be indexed to the {002} planes, as shown in Figure 10. These spots should be absent in the normal spinel structure as evidenced in Figure 2a because of the body diagonal glide symmetry. The presence of the 002 spots suggests a structural transition arising from the possible migration of cations during oxidation from Ni^{2+} to Ni^{4+}.

Figure 11 shows the ex situ XRD patterns of $Li_xNi_{0.5}Mn_{1.5}O_4$ at each state of charge. When charged to $x = 0.75$, another cubic phase was observed, and this new secondary cubic phase became dominant with diminishing pristine cubic phase at $x = 0.5$. Subsequent Li^+ deintercalation over 50% resulted in another cubic phase, and this third cubic phase was dominant at the fully charged state. Changes in the lattice parameter during the first charging process are also illustrated in Figure 9 (open symbols). The three cubic phases have lattice parameters of 8.16, 8.08, and 7.99 Å for the pristine, second, and third cubic phases, respectively. From these results, it is confirmed that $LiNi_{0.5}Mn_{1.5}O_4$ shows topotactic phase transitions among three different cubic phases.[22]

TEM observations were also performed for the $Li_xNi_{0.5}Mn_{1.5}O_4$ ($P4_332$) electrode during Li^+ extraction.

(22) Okada, M. In *Functional Chemistry Series of Electron and Ions, 'Next Generation Lithium Secondary Batteries'*; Tamura, E., Ed.; NTS Publisher: Tokyo, 2003; Vol. 3, p 156 (in Japanese).

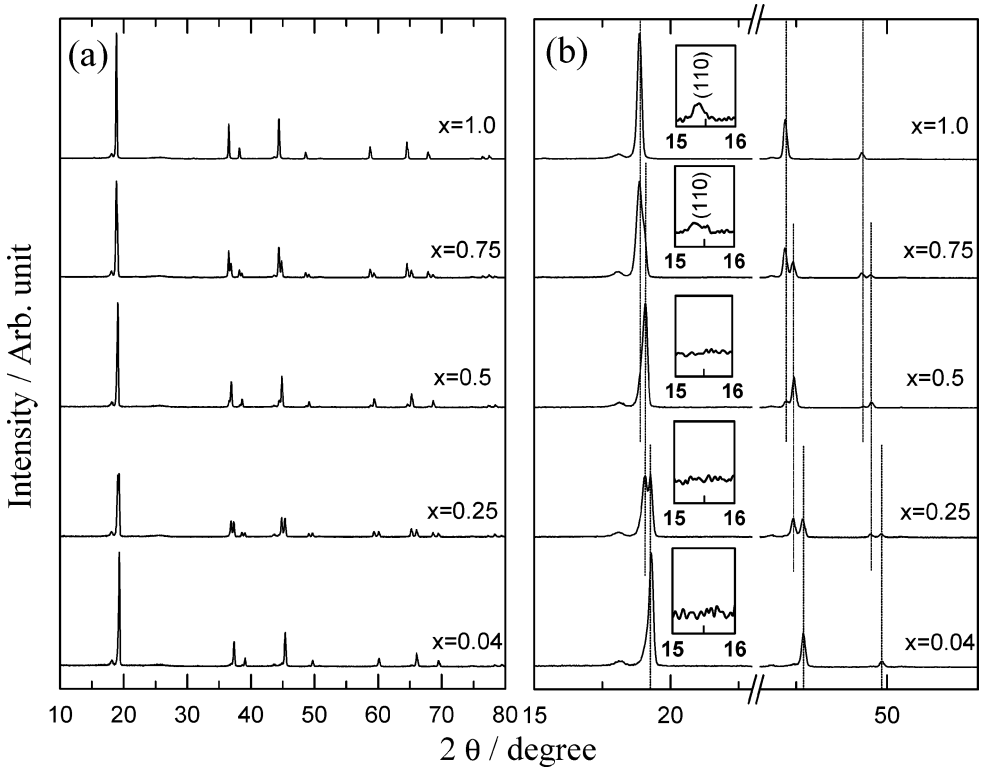

Figure 11. Ex situ X-ray diffraction (XRD) patterns of $Li_xNi_{0.5}Mn_{1.5}O_4$ ($P4_332$) electrodes at different states of charge.

Figure 12a shows the electron diffraction pattern of $Li_{0.5}Ni_{0.5}Mn_{1.5}O_4$. Compared to the pattern for the pristine $LiNi_{0.5}Mn_{1.5}O_4$ material in Figure 2b, the superlattice peaks stemming from the ordering of Ni and Mn have nearly disappeared when Li^+ was extracted, having diffraction patterns similar to that of the spinel ($Fd\bar{3}m$) in Figure 2a. This result is consistent with the XRD data (inset in Figure 1lb), which show the disappearance of the (110) reflection. This result suggests that Li extraction from the $Li_xNi_{0.5}Mn_{1.5}O_4$ ($P4_332$) structure leads to a disordering of the Ni and Mn ions with the structural transformation from $P4_332$ to spinel $Fd\bar{3}m$, which showed the intermediate second cubic phase. At the fully charged state, however, the $Li_{0.04}Ni_{0.5}Mn_{1.5}O_4$ electrode showed a structure similar to that of $Li_{0.04}Ni_{0.5}Mn_{1.5}O_{4-\delta}$ showing extra 002 spots in Figure 12b.

Compared to $LiNi_{0.5}Mn_{1.5}O_{4-\delta}$, which has a one-step phase transition between two cubic phases, $LiNi_{0.5}Mn_{1.5}O_4$ would experience a much greater strain during cycling, originating from the two-step phase transitions between three cubic phases, especially for the high-rate performance. At the low rate, however, it seems that Li^+ intercalation/deintercalation is slow enough to complete the phase transitions among three cubic phases, which, in turn, gives rise to the good cycling performance at 30 and 55 °C, as shown in Figures 3c and 4c.

To investigate structural changes during cycling, the XRD patterns of the $LiNi_{0.5}Mn_{1.5}O_{4-\delta}$ and $LiNi_{0.5}Mn_{1.5}O_4$ electrodes were measured in the fully discharged state after 50 cycles. Figure 13a shows the XRD patterns of $LiNi_{0.5}Mn_{1.5}O_{4-\delta}$ ($Fd\bar{3}m$) electrodes discharged at rates of $^1/_7$C and 3C at 30 and 55 °C (Both were charged at the $^1/_7$C rate). From the XRD results, it can be seen that no notable phase transition occurred during electrochemical cycling for the $LiNi_{0.5}Mn_{1.5}O_{4-\delta}$ material (Figure 13a). From the similar XRD patterns in Figure 13a, it was shown that the original spinel structure having

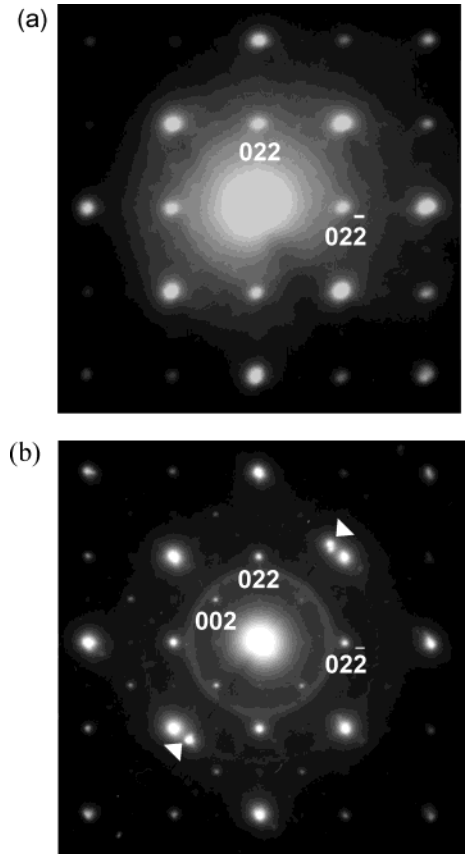

Figure 12. Ex situ electron diffraction patterns in the 100 zone for the $P4_332$ electrode: (a) $Li_{0.5}Ni_{0.5}Mn_{1.5}O_4$ and (b) $Li_{0.04}Ni_{0.5}Mn_{1.5}O_4$ (the spots indicated by the arrow in part b were generated from a overlapping crystal and are not part of the 100 diffraction pattern). The weak $0kl$ extra spots with k and $l \neq 2n$ in part b arose from multiple scattering.

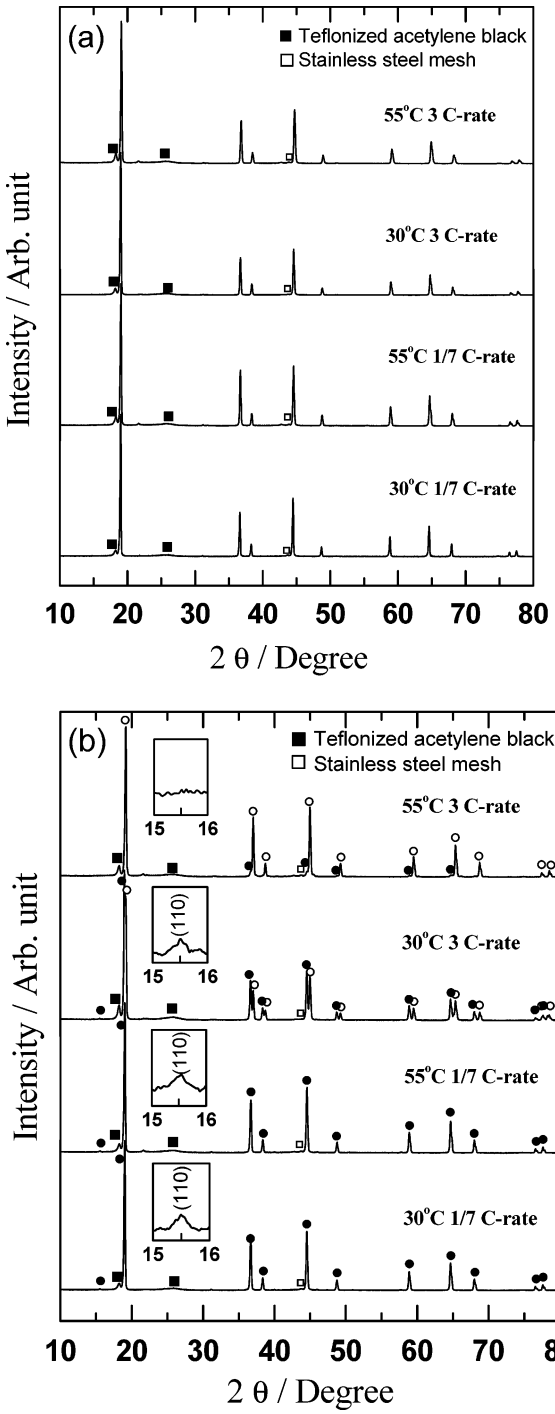

Figure 13. X-ray diffraction (XRD) patterns of electrodes after 50 cycles under various conditions. (a) $LiNi_{0.5}Mn_{1.5}O_{4-\delta}$ ($Fd\bar{3}m$) electrodes and (b) $LiNi_{0.5}Mn_{1.5}O_4$ ($P4_332$) electrodes (●, pristine primitive cubic phase; ○, newly formed cubic phase).

the $Fd\bar{3}m$ space group was maintained upon cycling regardless of the cycling conditions. This result confirms the conclusion that $LiNi_{0.5}Mn_{1.5}O_{4-\delta}$ ($Fd\bar{3}m$) undergoes a reversible phase transition during cycling even under severe conditions (55 °C, 3C rate).

Figure 13b shows the XRD patterns of the electrodes after 50 cycles for the $LiNi_{0.5}Mn_{1.5}O_4$ ($P4_332$) material. $LiNi_{0.5}Mn_{1.5}O_4$ electrodes cycled at the low rate ($^1/_7$C rate) maintained the pristine primitive cubic structure ($P4_332$) after 50 cycles at 30 and 55 °C. When the $LiNi_{0.5}Mn_{1.5}O_4$ electrodes were cycled at a rate of 3C, however, quite different XRD patterns were observed at 30 and

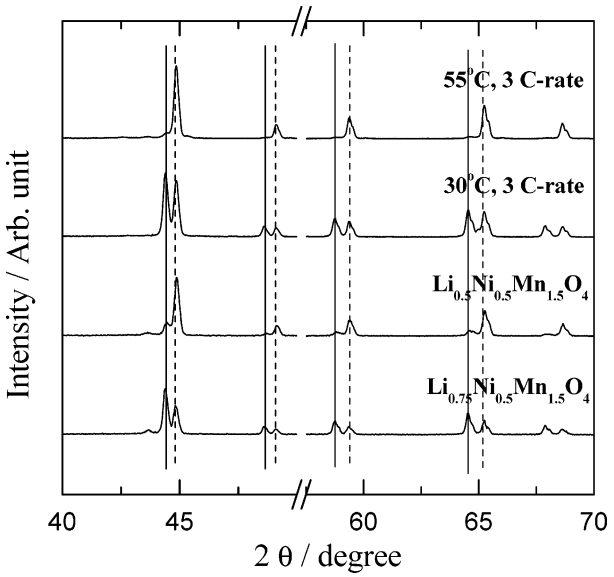

Figure 14. Comparison of the XRD profiles between after-cycled electrode (30 and 55 °C, $P4_332$) and ex situ XRD patterns ($x = 0.5$ and 0.75).

55 °C (Figure 13b). Interestingly, the electrode cycled at 30 °C at a rate of 3C exhibited another cubic phase even at the fully discharged state. Moreover, when the electrode was cycled at the 3C rate at 55 °C, the fraction of original cubic phase decreased considerably, whereas the newly formed cubic phase increased, as can be seen in Figure 13b.

The XRD patterns of the $LiNi_{0.5}Mn_{1.5}O_4$ ($P4_332$) electrodes cycled at the 3C rate are compared with the ex situ XRD patterns of $Li_xNi_{0.5}Mn_{1.5}O_4$ ($P4_332$) in Figure 14. The solid and dotted lines in this figure indicate the pristine and second cubic phases, respectively, of $LiNi_{0.5}Mn_{1.5}O_4$ ($P4_332$). The newly formed cubic phase after high-rate cycling exactly corresponds to the second cubic phase of $LiNi_{0.5}Mn_{1.5}O_4$ ($P4_332$), as indicated by the dotted line. The $LiNi_{0.5}Mn_{1.5}O_4$ electrode cycled at 30 °C at a rate of 3C exhibits XRD patterns similar to those of the $Li_{0.75}Ni_{0.5}Mn_{1.5}O_4$ electrode, meaning that the cycled electrode can be identified as $Li_xNi_{0.5}Mn_{1.5}O_4$ ($x < 0.75$). The $Li_{0.5}Ni_{0.5}Mn_{1.5}O_4$ electrode cycled at 55 °C has XRD patterns similar to those of $Li_{0.5}Ni_{0.5}Mn_{1.5}O_4$, meaning that the electrode can be presented as $Li_xNi_{0.5}Mn_{1.5}O_4$ ($x < 0.5$). These results indicate that Li ions could not fully intercalated into the $Li_xNi_{0.5}Mn_{1.5}O_4$ host structure on discharge, and therefore, the intermediate cubic phase such as $Li_xNi_{0.5}Mn_{1.5}O_4$ ($x < 1$) remained at the fully discharged state upon discharge at the 3C rate. In fact, the $P4_332$ electrode cycled at 30 and 50 °C at the rate of 3C exhibited a low discharge capacity compared to the $LiNi_{0.5}Mn_{1.5}O_{4-\delta}$ ($Fd\bar{3}m$) electrode, as depicted in Figures 3 and 4, which resulted from the low structural reversibility of the $Li_xNi_{0.5}Mn_{1.5}O_4$ phase at the high rate of 3C.

Figure 15a and b shows the electron diffraction patterns from two different particles in 100 and 011 zones, respectively, after cycling of the $LiNi_{0.5}Mn_{1.5}O_4$ ($P4_332$) electrode at a rate of 3C. Comparing Figure 15a with the pattern from the as-prepared sample in Figure 2b, the relative intensity of the superlattice peaks has noticeably decreased. In the case of Figure 15b, the

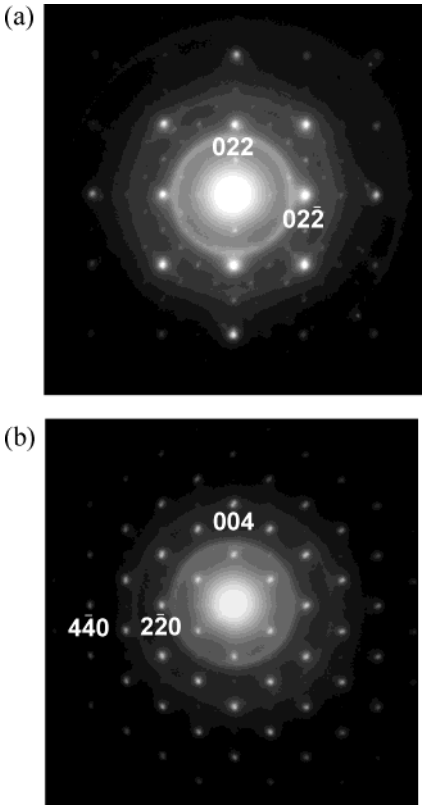

Figure 15. Electron diffraction patterns from two different particles in the (a) [100] and (b) [011] zones after cycling of the $LiNi_{0.5}Mn_{1.5}O_4$ ($P4_332$) electrode at a rate of 3C.

superlattice peaks were hardly discernible. It appears that, when the $LiNi_{0.5}Mn_{1.5}O_4$ ($P4_332$) electrode is cycled at a sufficiently high rate, complete ordering of the cations is not quite achieved, leading to an intermediate cubic structure as evidenced from the electron diffraction patterns.

Conclusions

Stoichiometric and nonstoichiometric $LiNi_{0.5}Mn_{1.5}O_{4-\delta}$ materials with two different structures ($P4_332$ and $Fd\bar{3}m$) were synthesized and comparatively studied. By additional heating at 700 °C, Ni and Mn in $LiNi_{0.5}Mn_{1.5}O_4$ ordered and changed the structure from face-centered spinel ($Fd\bar{3}m$) to primitive simple cubic ($P4_332$), as evidenced by XRD and SAED. $LiNi_{0.5}Mn_{1.5}O_4$ ($Fd\bar{3}m$) exhibited stable cyclability upon cycling at a high rate, compared to that of $LiNi_{0.5}Mn_{1.5}O_4$ ($P4_332$). Area-specific impedance (ASI) measurements showed that $LiNi_{0.5}Mn_{1.5}O_4$ with the $P4_332$ structure has a higher resistance than that with the $Fd\bar{3}m$ structure during delithiation. $LiNi_{0.5}Mn_{1.5}O_{4-\delta}$ ($Fd\bar{3}m$) undergoes a one-step phase transition, and $LiNi_{0.5}Mn_{1.5}O_4$ ($P4_332$) undergoes the two-step phase transition. XRD and SAED for the cycled $LiNi_{0.5}Mn_{1.5}O_4$ ($P4_332$) electrodes showed that the reversible two-step phase transition was not completed at a high rate of 3C. Meanwhile, the $LiNi_{0.5}Mn_{1.5}O_4$ ($Fd\bar{3}m$) electrode having the one-step phase transition exhibited good reversibility even upon high-rate cycling. From these results, it is confirmed that $LiNi_{0.5}Mn_{1.5}O_4$ with the space group of $Fd\bar{3}m$ has superior electrochemical behavior and structural reversibility compared to $P4_332$.

Acknowledgment. This work was supported by KOSEF through the Research Center for Energy Conversion and Storage.

CM035050S